

**Oligomeric phosphate clusters in macrocyclic channels**

Journal:	<i>CrystEngComm</i>
Manuscript ID	CE-COM-06-2022-000756.R1
Article Type:	Communication
Date Submitted by the Author:	06-Sep-2022
Complete List of Authors:	Bowman-James, Kristin; The University of Kansas, Department of Chemistry Pramanik, Subhamay; The University of Kansas, Chemistry Day, Victor; The University of Kansas, Chemistry Thordarson, Pall; The University of New South Wales, School of Chemistry

COMMUNICATION

Oligomeric phosphate clusters in macrocyclic channels

Subhamay Pramanik,^a Pall Thordarson,^b Victor W. Day^a and Kristin Bowman-James^{*a}Received 00th January 20xx,
Accepted 00th January 20xx

DOI: 10.1039/x0xx00000x

A 36-membered macrocycle, H_31^{3+} , crystallizes with a mixture of five phosphates with valences HPO_4^{2-} , $H_2PO_4^-$, and H_3PO_4 . The macrocycles form sandwich-like channels for clusters of six phosphates interconnected through oligomeric chains of water-linked phosphates and phosphoric acid molecules. Binding studies indicate 3:1 phosphate:macrocycle associations in keeping with 6:2 phosphate:macrocycle “sandwiches.”

Earth's rapidly depleting sources of phosphorus, a crucial element for global well-being, have become an issue of great concern.¹⁻⁴ Current phosphorus resources come mainly from what is known as “phosphate rock”, mineral deposits with large concentrations of inorganic phosphate. Organic-based phosphates, another potential source of phosphorus, are also prevalent throughout Nature, and are prominent in key metabolic and biosynthetic processes.^{5,6} Contrary to its important biological roles, overabundance of phosphate can negatively affect the environment. For example, run-off of ground water contaminated by over-usage of phosphate-containing fertilizers enables the growth of algal blooms harmful to aquatic inhabitants, ultimately affecting fresh-water resources.²⁻⁴

In order to address the serious concerns involving the worldwide phosphorus reserves, supramolecular chemists are focused on obtaining a better understanding of the chemistry of phosphate-containing molecules and ions.¹ For example, of all the oxoanions, phosphates in particular, have a natural propensity to self-associate, which makes their chemistry all the more complex.⁷⁻¹⁵ Furthermore, it is becoming increasingly apparent that oligomerization is not just limited to phosphate, but also to other important anions.¹⁶⁻¹⁹ Hence, inter-anionic

interactions have become an important area of supramolecular focus.

Recently we identified a 36-membered mixed amide/amine based macrocycle (H_31^{3+} , Figure 1(a)) that formed sandwich-like 2:1 host:guest complexes with two stereoisomers of the class of polyanions known as inositol hexaphosphates (IP_6).²⁰ The most prevalent of these, phytate, plays major roles in plant metabolism.²¹⁻²³ Not only is it found in plants, it is also a large component of the organophosphates found in soils.

Here we report the structure of a sandwich-like host-guest complex of a hexaphosphate cluster with H_31^{3+} (Figure 1(b)) that is structurally reminiscent of the above-mentioned IP_6 structures. The spatial arrangement and separations of phosphate groups within this pseudo-sandwich are generated in the crystal by a crystallographic inversion center. The resulting arrangements in the phosphate hexamer are quite similar with those observed in the IP_6 structures, indicating a similar binding motif for the “discrete” phosphates.

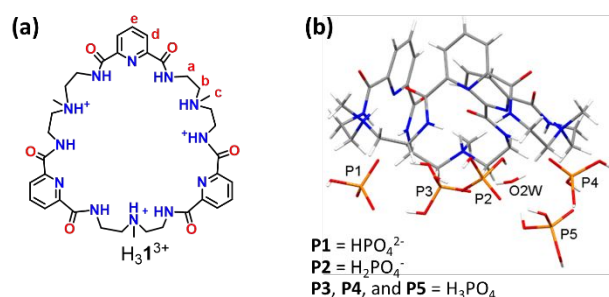


Fig. 1. (a) ChemDraw diagram of the positively-charged macrocycle, H_31^{3+} , and (b) a perspective view of the asymmetric unit of a single host, H_31^{3+} , the protonated phosphates, and O2W. O1w, that lies outside the complex, is not shown.

The amide-based macrocycle **1** was synthesized from N-methyl-2,2'-diaminodiethylamine and 6-dimethyl-pyridine dicarboxylate.²⁰ The phosphate cluster was obtained by slow addition of H_3PO_4 to a methanol solution of **1**. Thin platelets were obtained on slow evaporation of a $H_2O:MeOH:CH_3CN$ (1:2:1) solution. The cluster crystallized as a mixed-valent salt, $[(H_31)(HPO_4)(H_2PO_4)] \cdot 3H_3PO_4 \cdot 2H_2O$, with one HPO_4^{2-} (P1), one

^a Department of Chemistry, University of Kansas, Lawrence, Kansas 66045, United States, E-mail: kbjames@ku.edu.

^b School of Chemistry, The Australian Centre for Nanomedicine and the UNSW RNA Institute, The University of New South Wales, Sydney, NSW 2052, Australia. E-mail: p.thordarson@unsw.edu.au

†Electronic Supplementary Information (ESI) available: For Materials, Instrumentation, Crystallization, Spectroscopic analysis and X-ray crystallographic studies (CCDC 2113443). See DOI: 10.1039/x0xx00000x

H_2PO_4^- (P2), and three neutral H_3PO_4 s (P3, P4, and P5) (Fig. 1(b)). While a cluster arrangement with three H_2PO_4^- ions and two H_3PO_4 molecules within the macrocycles might be more likely to be observed and indeed, probably exists in solution, the structure refinement clearly indicated the mixed valent phosphates described above. Besides being able to locate phosphate hydrogen atoms in a difference Fourier and refining their parameters in least-squares refinement cycles, significant elongation is observed for protonated P-O bonds as expected. The equilibrium solution could contain all three species to some extent given the ability of protons to transfer from one anion to another close neighbor, and this particular crystalline arrangement could favour such a combination, either as the crystal begins to form or after it has formed through proton migration.

Six phosphates lie within the sandwich-like host cavity (P1, P2, and P3, and their symmetry-related counterparts P1', P2', and P3') (Figure 2(a) and (b)). Direct P-OH...O-P interactions range from 2.52–2.65 Å. Two water molecules (H_2O_2 and $\text{H}_2\text{O}_2'$) link the acids, P3 and P3', to the monoanions, P2 and P2'. The acids, P3/P3', also form two P-OH...O hydrogen bonds to the dianion P1/P1'. The other two neutral phosphoric acids, P4 and P5, lie at the outer edges of the macrocycles, as does a disordered water, H_2O_1 , in which the oxygen was modeled over two positions with occupancies of 80 and 20%. The two symmetry-related triphosphate chains, P1-P3 and P1'-P3', are attached by two hydrogen bonds between P1 and P2' and its symmetry corollary P2 to P1'.

Only the oxygen atoms of the anionic phosphates, P1 and P2, and one of the external phosphoric acids (P4) are directly bound to the chelating pyridine amide units (Fig. 2(c)). The amides of two of the pyridines form chelates with the dianion, P1, and the acid, P4, while P1 is only hydrogen bonded to the third pyridine through one of its amides.

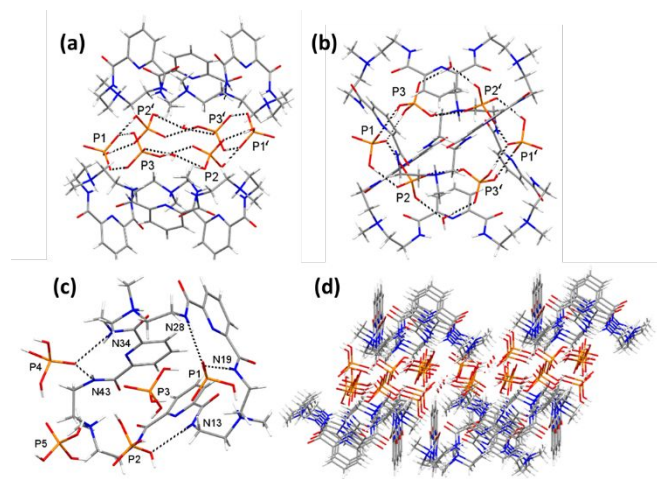


Fig. 2 (a) Side perspective view of the hexaphosphate cluster with water bridges between P2/P2' and P3/P3'; (b) overhead view (90° rotation) of (a); (c) view showing hydrogen bonds between P1, P2, and the external P4 to $\text{H}_3\text{1}^{3+}$; and (d) extended view along the crystallographic *c* axis of channel-like oligomeric chains of phosphates and waters between macrocyclic walls.

When extended, the hosts line channels for oligomeric phosphate-water chains with P-OH...OH₂ and H-OH...O-P O---O distances ranging from 2.510(3) – 2.659(3) Å (Fig. 2(d)). Extended in three dimensions, intricate phosphate/phosphoric acid lattice networks are revealed, as seen without the macrocycles (Fig. 3(a)). We were unsuccessful in attempts to fit our inter-phosphate interactions to one of the patterns noted by Custelcean and co-workers for monohydrogen phosphates.¹¹ Complications in this effort were the presence of both the mono- and di-hydrogen phosphates as well as the presence of the water molecules. Nonetheless, both direct P-OH...O-P hexamer and decamer patterns can be detected (Fig. 3(b) and (c)). In addition, a vertical linear array of direct phosphate-phosphate interactions can be seen on the left and right sides of Fig. 3(a): P5-P2=P1-P4-P5-P4=P2=P1. Addition of the macrocycles to the picture with color-coding for the phosphates of different valences accentuates the motif of interspersed anions/acids/water chains (Fig. 3(d) and (e)).

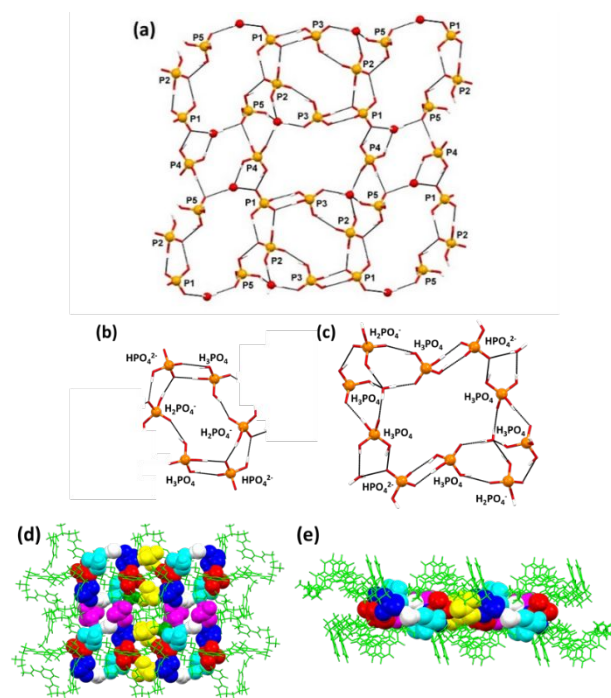


Fig. 3 (a) View of a phosphate-water network approximately 1.5 unit cell in length along *c* without the macrocycles (phosphorus atoms displayed as balls); (b) view of the isolated hexamer of P1, P2, P3, P1, P2, P3 (middle of (a), top and bottom); (c) view of the isolated decamer P2, P5, P4, P1, P3, P2, P5, P4, P1, and P3 (center of (a)); (d) and (e) two views of the phosphate network in (a) with color-coded, space-filled phosphates, phosphoric acids, and waters, plus added (light green sticks) macrocycle hosts. P1 (blue, HPO_4^{2-}); P2 (red, H_2PO_4^-); P3 (yellow, H_3PO_4); P4 (magenta, H_3PO_4); P5 (cyan, H_3PO_4) and H_2O (white, $\text{H}_2\text{O}_1\text{W}$ and $\text{H}_2\text{O}_2\text{W}$).

The sandwiched phosphates within the macrocyclic hosts are structurally similar to those found in our recent crystal structures of phytate and another more symmetrical IP_6 polyphosphate, the *scyllo* stereoisomer. As noted in the introduction, phytate and the *scyllo*- IP_6 were found to be sandwiched between two $\text{H}_3\text{1}^{3+}$ macrocycles. The overhead view of the phosphate cluster (shown in Fig. 2(b)) is quite similar to that of the *scyllo*- IP_6 (Fig. 4(a)).²⁰ An overlay of the

H_31^{3+} complex with *scyllo*-IP₆, $2(H_31^{3+})(scyllo-IP_6^{6-})$, with the hexaphosphate cluster, further supports the similarities (Fig. 4(b)) (rms deviation for P atoms = 1.24 Å) (Fig. 4(b) and Fig. S1(a) and (b), ESI[†]), which is slightly better than that of the phytate (*myo*-IP₆) with $2H_31^{3+}$ cations (Fig. S1(c) and (d), ESI[†]). The rms deviations of the overlays of the hexaphosphate cluster with our two recent structures of the octasodium *scyllo*-IP₆ and tripotassium *myo*-IP₆ salts (rms = 1.0 Å and 1.22 Å, respectively) (Fig. S2(a) and (b), ESI[†]).^{24,25}

Binding interactions of H_31^{3+} with the tetrabutylammonium (TBA) salt of dihydrogen phosphate, $H_2PO_4^-$ were examined by ¹H and ³¹P NMR studies in DMSO-*d*₆. On gradual addition of (TBA)(H₂PO₄) (20 mM) to the solution of **1** (2 mM), the amide NH signal shifted downfield from 9.16, broadening after the addition of about one equiv. (9.8 ppm). At about 3 equiv. of H₂PO₄⁻ (10.5 ppm), the signal began to sharpen and continued to sharpen while slowly shifting downfield to 10.8 ppm at 10 equiv. H₂PO₄⁻ (Fig 5(a) and Fig. S3, ESI[†]). The resulting binding curve (Fig. 5(b)) was indicative of 1:3 H₃1:phosphate binding as seen in the crystal structure.

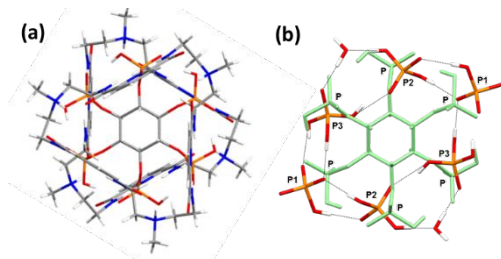


Fig. 4 (a) Overhead perspective sandwich view of $2H_31^{3+}$ ions with *scyllo*-IP₆⁶⁻ and (b) overlay of the *scyllo*-IP₆⁶⁻ with the phosphates in the hexaphosphate cluster (IP₆ bonds light green).

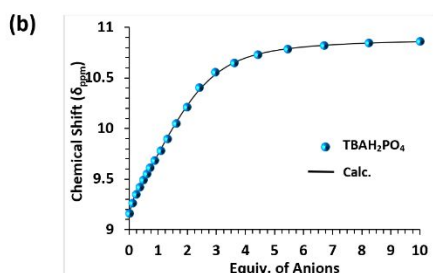
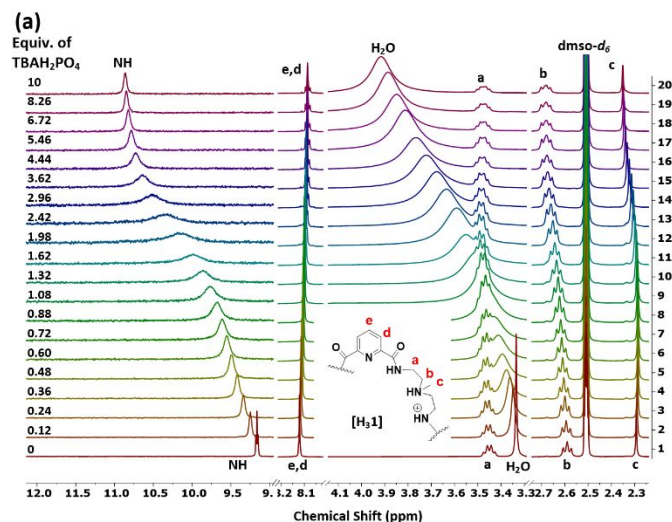


Fig. 5 (a) ¹H chemical shift changes of **1** (2 mM) with increasing concentration of (TBA)(H₂PO₄) (20 mM) in DMSO-*d*₆ (400 MHz, 298 K) and (b) binding isotherm of the amide NH protons of **1** as a function of added aliquots of (TBA)(H₂PO₄). Solid line corresponds to the cooperative 1:3 binding model used here.

The amide chemical shifts were evaluated for 1:3 macrocycle:phosphate binding using Matlab for both a full and non-cooperative binding model.^{26,27} Data were observed to fit best to a 1:3 binding model with some positive cooperativity. Since the simpler, non-cooperative model could not be ruled out, the chemical shifts of the four macrocycle proton resonances were also evaluated (Section S4 and Table S1 for further details, ESI[†]). Binding constants for this model were $K_1 = 968$, $K_2 = 68,204$, and $K_3 = 1,024 M^{-1}$, which, after correcting for statistical factors, correspond to $\Delta G_1 = -6.2$, $\Delta G_2 = -12.0$, and $\Delta G_3 = -8.6 kJ mol^{-1}$, respectively, indicating positive cooperativity.

The ³¹P NMR titration of the reverse addition of the host **1** to a solution of (TBA)(H₂PO₄) revealed an initial downfield shift of the signal, with a reversal at 0.34 equivalents of **1**, at a 3:1 phosphate:1 ratio. The signal then shifted back upfield to about 0.5 ppm (Fig. 6(a)). This 3:1 pattern is consistent with what we observe in the ¹H NMR as well as in the crystal structure, i.e. a 3:1 H₂PO₄⁻:**1** ratio. Downfield followed by upfield trends have been attributed to cluster/oligomer formation.¹⁰

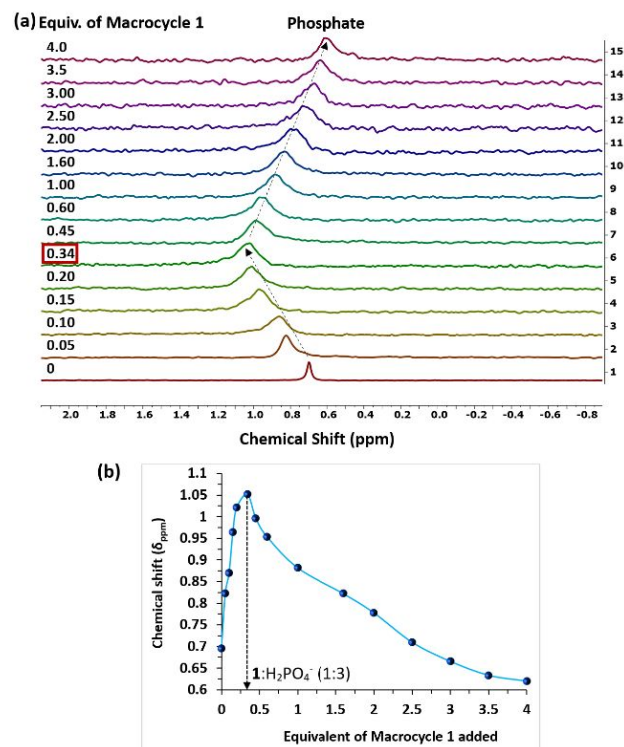


Fig. 6 (a) ³¹P NMR spectra showing chemical shift changes of (TBA)(H₂PO₄) (10 mM) with increasing aliquots of macrocycle **1** (40 mM) in DMSO-*d*₆ (400 MHz, 298 K); and (b) binding isotherm of the phosphate ³¹P signals as a function of added aliquots of **1**.

The ESI-MS spectrum of a solution of crystals of **1** shows the appearance of a parent peak (*m/z*) of 843.30 equivalent to **1** + H₃PO₄, plus signals at 941.32, 1039.32, 1137.31 and 1243.56 with spacing of nearly 98 Dalton (MW H₃PO₄) (Fig. S4, ESI[†]).

Additional peaks were also observed at 1685.80, 1783.82, 1881.82, 1979.97 and 2079.07, ultimately corresponding to the formation of a hexamer cluster sandwiched between two macrocycles $[(1)_2 \cdot (H_3PO_4)_6 + H]^+$ (Fig. 7).

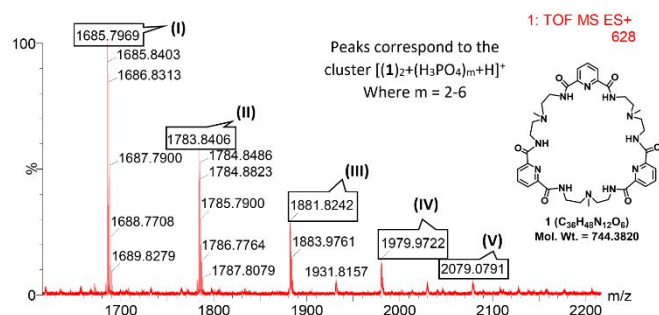


Fig. 7 ESI-MS (+ve) spectrum of a solution of the crystals showing peaks corresponding to $[(1)_2 + (H_3PO_4)_m + H]^+$ cluster with m/z : (I) 1685.7969, $[(1)_2 + (H_3PO_4)_2 + H]^+$; (II) 1783.8406, $[(1)_2 + (H_3PO_4)_3 + H]^+$; (III) 1881.8242, $[(1)_2 + (H_3PO_4)_4 + H]^+$; (IV) 1979.9722, $[(1)_2 + (H_3PO_4)_5 + H]^+$ and (V) 2079.0791, $[(1)_2 + (H_3PO_4)_6 + H]^+$ with constant spacing of 98 Da (molecular weight of H_3PO_4).

In conclusion, a 36-membered cationic macrocycle was found to shield a cluster of six “discrete” phosphates. The positioning of the phosphates was found to be in configuration quite similar to those observed in our previous report for the six phosphates in IP_6 covalently docked to inositol.²⁰ Yet, the clusters are also connected to neighboring clusters resulting in an oligomeric chain of phosphate clusters. These results illustrate the ability of macrocyclic hosts to orient/position their guests in similar patterns. In this instance, what is observed in the crystalline-state appears also to be observed in solution, where multiply-valent species are able to coexist. Ultimately, the structures of anion clusters are not necessarily random; rather, certain preferred supramolecular “coordination” tendencies seem to establish and stabilize common motifs.

Contributions of Authors

SP: experimental investigations, methodology. PT: binding analysis, methodology. VWD: crystal structure and analysis. KBJ: conceptualization, writing and reviewing.

Conflicts of interest

There are no conflicts to declare.

Acknowledgements

The authors thank the National Science Foundation (CHE-1710535) for support of the binding studies and comparisons to the inositol hexaphosphates and (CHE-0923449) for the purchase of the X-ray diffractometer. The crystallizations and cluster/oligomerization studies were supported by the Chemical Sciences, Office of Basic Energy Sciences, Office of Science, U.S. Department of Energy (Grant

DE-SC0018629). The authors would also like to thank Dr. Nigam Rath for discussions concerning the crystal structure.

Notes and references

- J. J. Elser and M. S. Platz, *Closing the Human Phosphorus Cycle*, NSF FEWS Workshop Report, Arlington, VA, June 8-9, 2015.
- D. Cordell and S. White, *Ann. Rev. Environ. Resour.*, 2014, **39**, 161–188.
- J. J. Elser and E. Bennett, *Nature*, 2011, **478**, 29–31.
- H. P. Jarvie, A. N. Sharpley, D. Flaten, P. J. A. Kleinman, A. Jenkins and T. Simmons, *J Environ. Qual.*, 2015, **44**, 1049–1062.
- A. K. H. Hirsch, F. R. Fischer and F. Diederich, *Angew. Chem. Int. Ed.*, 2007, **46**, 338–352.
- A. E. Hargrove, S. Nieto, T. Zhang, J.; Sessler, and E. V. Anslyn, *Chem. Rev.*, 2011, **111**, 6603–6782.
- E. M. Fatila, M. Pink, E. B. Twum, J. A. Karty and A. H. Flood, *Chem. Sci.*, 2018, **9**, 2863–2872.
- R. Chutia, S. K. Dey and G. Das, *Cryst. Growth Des.*, 2015, **15**, 4993–5001.
- O. A. Gerasimchuk, S. Mason, J. M. Llinares, M. Song, N. W. Alcock and K. Bowman-James, *Inorg. Chem.*, 2000, **39**, 1371–1375.
- M. A. Hossain, M. Isiklan, A. Pramanik, M. A. Saeed and F. R. Fronczek, *Cryst. Growth Des.*, 2012, **12**, 567–571.
- A. Rajbanshi, S. Wan and R. Custelcean, *Cryst. Growth Des.*, 2013, **13**, 2233–2237.
- B. Wu, C. Huo, S. Li, Y. Zhao and X.-J. Yang, *Z. Anorg. Allg. Chem.*, 2015, **641**, 1786–1791.
- D. Mungalpara, A. Valkonen, K. Rissanen, and S. Kubik, *Chem. Sci.*, 2017, **8**, 6005–6013.
- F. Zapata, L. González, a. Bastida, D. Bautista, and A. Caballero, *Chem. Commun.*, 2020, **56**, 7084 – 7087.
- E. Saridakis, E.-M. Kasimati, K. Yannakopoulou, and I. M. Mavridis, *Chem. Commun.*, 2022, **58**, 5300–5303.
- S.-O. Kang, T. S. Johnson, V. W. Day and K. Bowman-James, *Supramol. Chem.*, 2018, **30**, 305–314.
- Qing He and J. L. Sessler, *Chem*, 2018, **4**, 46–93.
- N. G White, *CrystEngComm*, 2019, 4855–4858.
- W. Zhao, A. H. Flood, and N. G. White, *Chem. Soc. Rev.*, 2020, **49**, 7893–7906.
- S. Pramanik, V. W. Day and K. Bowman-James, *Chem. Commun.*, 2020, **56**, 3269–3272.
- V. Raboy, *Phytochem.* 2003, **64**, 1033–1043.
- M. Bennett, S. M. N. Onnebo, C. Azevedo, and A. Saiardi, *Cell. Mol. Life Sci.*, 2006, **63**, 552–564.
- C. Kremer, J. Torres, A. Bianchi, M. Savastano and C. Bazzicalupi, *Coord. Chem. Rev.*, 2020, **419**, 213403–213421.
- S. Kaur, S. Pramanik, V. W. Day, and K. Bowman-James, *Dalton Trans.*, 2021, **50**, 480–484.
- M. Reinmuth, S. Pramanik, J. T. Douglas, V. W. Day, and K. Bowman-James, *Eur J. Inorg. Chem.* 2019, (Iss. 14), 1870–1874.
- P. Thordarson *Chem. Soc. Rev.*, 2011, **40**, 1305–1323.
- D. B. Hibbert and P. Thordarson, *Chem. Commun.*, 2016, **52**, 12792–12805.